

Characteristics of Vertical Ga_2O_3 Schottky Junctions with the Interfacial Hexagonal Boron Nitride Film

Venkata Krishna Rao Rama,* Ajinkya K. Ranade, Pradeep Desai, Bhagyashri Todankar, Golap Kalita, Hiroo Suzuki, Masaki Tanemura, and Yasuhiko Hayashi*



Cite This: *ACS Omega* 2022, 7, 26021–26028



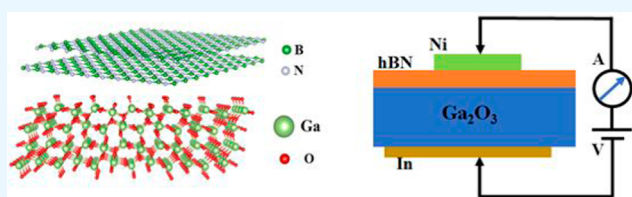
Read Online

ACCESS |

Metrics & More

Article Recommendations

ABSTRACT: We present the device properties of a nickel (Ni)–gallium oxide (Ga_2O_3) Schottky junction with an interfacial hexagonal boron nitride (hBN) layer. A vertical Schottky junction with the configuration Ni/hBN/ Ga_2O_3 /In was created using a chemical vapor-deposited hBN film on a Ga_2O_3 substrate. The current–voltage characteristics of the Schottky junction were investigated with and without the hBN interfacial layer. We observed that the turn-on voltage for the forward current of the Schottky junction was significantly enhanced with the hBN interfacial film. Furthermore, the Schottky junction was analyzed under the illumination of deep ultraviolet light (254 nm), obtaining a photoresponsivity of 95.11 mA/W under an applied bias voltage (−7.2 V). The hBN interfacial layer for the Ga_2O_3 -based Schottky junction can serve as a barrier layer to control the turn-on voltage and optimize the device properties for deep-UV photosensor applications. Furthermore, the demonstrated vertical heterojunction with an hBN layer has the potential to be significant for temperature management at the junction interface to develop reliable Ga_2O_3 -based Schottky junction devices.



INTRODUCTION

Gallium oxide (Ga_2O_3) with an ultrawide band gap (UWBG) has piqued the interest of researchers working on deep ultraviolet (UV) photonics and next-generation power electronic devices.^{1–5} Semiconductors based on UWBG Ga_2O_3 materials can withstand much higher critical electric fields (6–8 MV/cm) before avalanche breakdown than silicon-(Si), silicon carbide-(SiC), and gallium nitride (GaN)-based devices.^{1,6,7} Furthermore, Baliga's figure of merit presents the advantage of Ga_2O_3 for power switching applications over the Si (3000×), SiC (10×), and GaN (4×).^{8,9} It has been demonstrated that high-quality single-crystal Ga_2O_3 can be synthesized using melt growth techniques such as Czochralski, floating zone, and edge-defined film-fed growth (EFG).^{10–15} In addition, halide vapor phase epitaxy (HVPE), molecular beam epitaxy (MBE), and chemical vapor deposition (CVD) methods for growing high-quality Ga_2O_3 have been developed.^{16–25} Johnson's figure of merit (JFOM/power–frequency product) of Ga_2O_3 (3× of GaN)^{26,27} illustrates the potential benefit of using Ga_2O_3 in radio frequency (RF) devices. Chabak et al. have reported on the fabrication of the Ga_2O_3 MOSFET device using a thin and highly doped channel and achieving a drain-source current of 275 mA/mm at a drain to source bias of 10 V for that exhibited record-high $f_t/f_{max} = 5.1/17.1$ GHz.²⁸ However, it is expected that Ga_2O_3 devices will suffer from self-heating due to the poor thermal conductivity of the material. The device model demonstrates that a

homoepitaxial device suffers from an unacceptable junction temperature increase to 1500 °C at a power density of 10 W/mm, highlighting the importance of applying device-level thermal managements to individual Ga_2O_3 devices.^{29,30} In this case, the integration of thermal conducting materials with Ga_2O_3 -based devices may be critical for achieving dependable device performance.

The heterojunction and Schottky junction-based β - Ga_2O_3 devices are of great interest for the development of high-voltage devices and solar-blind UV photodetectors, considering the intrinsic n-type conductivity of β - Ga_2O_3 in the presence of unintentional dopants.^{25–31} The conventional Ga_2O_3 Schottky junction devices were studied with metal electrodes such as Au, Pt, and Ni, taking into account the metals' appropriate work function.^{32,33} Again, studies on metal–insulator–semiconductor (MIS)-based SBD devices have been conducted, owing to the benefit of lowering the reverse saturation current.^{34–36} The MIS-based SBD devices have been fabricated using insulating dielectric materials, such as SiO_2 , Si_3N_4 , Al_2O_3 , and so forth.^{35–37,40} The thermal stability of Ga_2O_3 Schottky contacts

Received: January 25, 2022

Accepted: May 18, 2022

Published: July 22, 2022



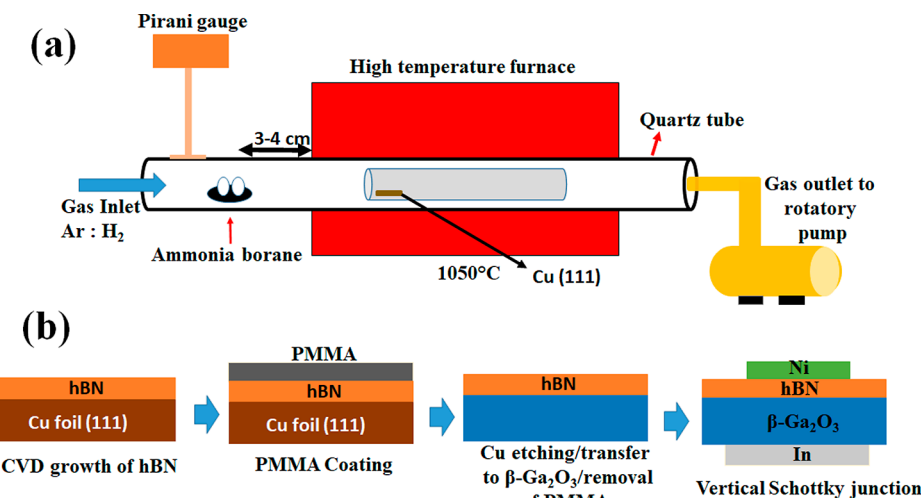


Figure 1. (a) Schematic diagram of the APCVD process for synthesis of the hBN film on Cu foil. (b) Transfer process of the CVD-synthesized hBN film for the fabrication of the Ni/hBN/β-Ga₂O₃/In heterojunction Schottky diode.

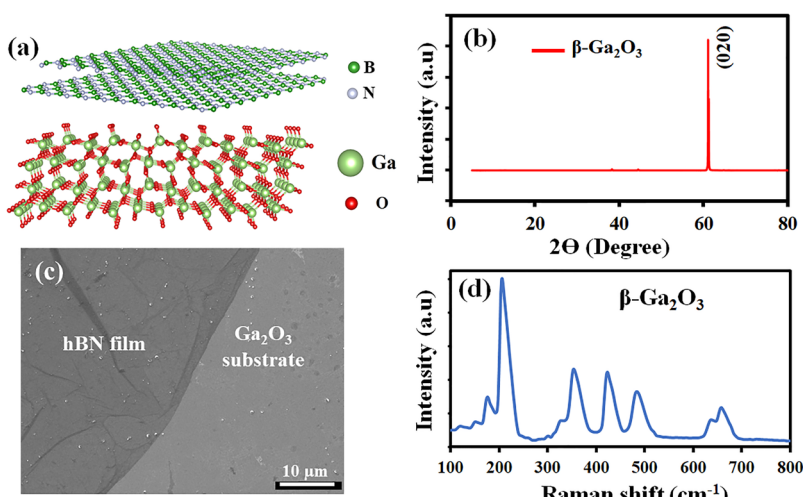


Figure 2. (a) Cross-sectional schematic diagram of the hBN and β -Ga₂O₃ heterostructure. (b) XRD pattern of the free-standing β -Ga₂O₃ substrate. (c) SEM image of the hBN film on the β -Ga₂O₃ substrate. (d) Raman spectra of the β -Ga₂O₃ sample.

is also an important aspect, for which materials with high melting temperatures and low reactivity with Ga₂O₃ are of significant interest.³⁷ Furthermore, controlling near-surface ion damage during sputtering deposition of a barrier layer/insulating dielectric^{7,40} is required. In this case, the CVD-synthesized chemically inert insulating hBN layer will be significant with much higher in-plane thermal conductivity for use in Ga₂O₃-based Schottky junctions.^{38,39}

Previously, we have demonstrated the integration of highly conducting graphene and copper iodide (γ -CuI) films with the β -Ga₂O₃ substrate for the fabrication of deep-UV photoresponsive devices.^{41,42} The fabrication of quasi-two-dimensional metal–insulator–semiconductor field-effect transistors was demonstrated by the mechanical transfer process of hBN and nanothin flakes of β -Ga₂O₃.⁴³ In contrast to previous reports, we show how to make a vertical Ni/ β -Ga₂O₃ Schottky junction with and without the hBN interfacial layer. The UWBG heterostructure of hBN and β -Ga₂O₃ can be significant due to the complementing electronic, chemical, and thermal properties of the materials. The following sections go over the specifics of hBN integration with the free-standing β -Ga₂O₃

substrate and the fabrication of a vertical Schottky junction. We discovered that the hBN interfacial film can be used to control the device's turn-on voltage and current density.

EXPERIMENTAL SECTION

The hBN film was synthesized on recrystallized Cu (111) foil by the atmospheric pressure CVD (APCVD) as reported previously by the research group (Figure 1a).^{44–46}

For this experiment, ammonia borane (10 mg) is used as a precursor and placed atop a magnetic boat, which was placed inside the tube about 20 cm away from the furnace to avoid precursor loss before the deposition step. The furnace was set at a high temperature of 1050 °C for the growth of the hBN film on the Cu surface. During the deposition step, the gas flow into the chamber was changed by the addition of argon gas with a flow rate of 98 sccm, and the flow rate of hydrogen gas was reduced to 2 sccm, and the mixed gas flow was 98:2 of Ar/H₂. To achieve vaporization of ammonia borane, the precursor is brought close to the furnace using a magnet at 3 cm away from the furnace, as shown in the schematic diagram (Figure 1a). The deposition step was set for 40 min, allowing for the

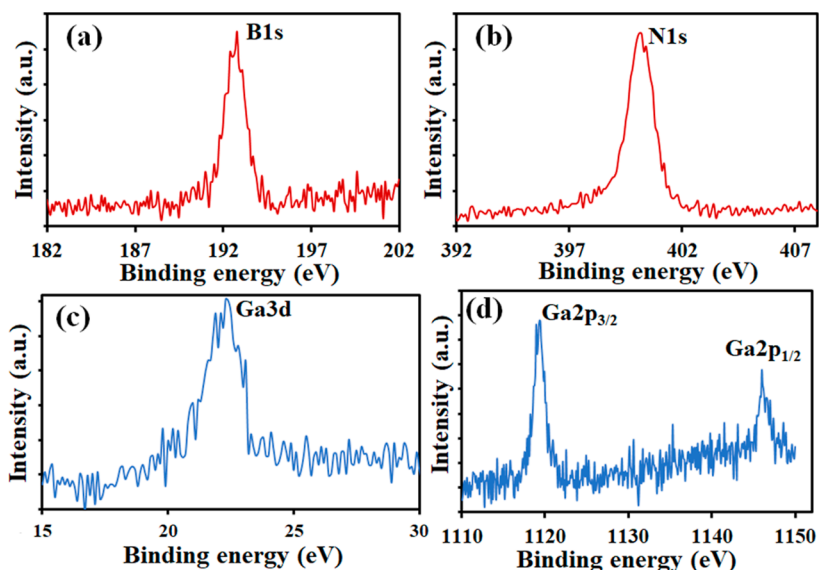


Figure 3. XPS spectra for the fabricated hBN/β-Ga₂O₃ heterostructure sample. (a) B 1s spectra with a peak center at around 192.8 eV, (b) N 1s spectra with a peak center at 400.1 eV, (c) Ga 3d spectra with a peak center at 22.3 eV, and (d) Ga 2p_{3/2} and Ga 2p_{1/2} peaks with peak centers at 1119.4 and 1146.0 eV, respectively.

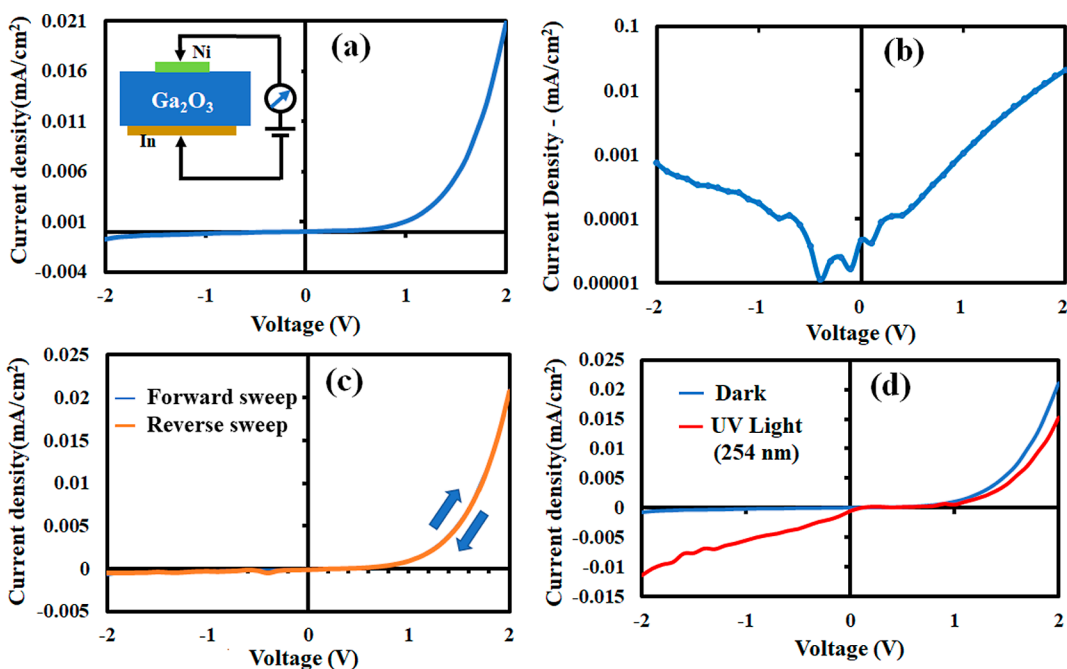


Figure 4. *J*–*V* characteristic of the Ni/β-Ga₂O₃/In Schottky junction: (a) *J*–*V* characteristic for the voltage range of 2 to −2 V (inset shows a schematic diagram of the fabricated device) and (b) log plot of the *J*–*V* curve. (c) *J*–*V* characteristics of the forward and reverse sweep for the voltage range of 2 to −2 V. (d) *J*–*V* curve under dark and deep-UV illumination (254 nm).

formation of an hBN layer on a Cu (111) substrate. Finally, the cooling step was completed by simultaneously switching the H₂ gas flow, partially opening the furnace, and moving the precursor approximately 20 cm away from the furnace to avoid a secondary deposition. After the reaction chamber was cooled to room temperature, the hBN-grown Cu foil was removed and subjected to a wet transfer process described in the previous reports.⁴⁴ An hBN/β-Ga₂O₃ stack was obtained by transferring the CVD-synthesized hBN film on the Ga₂O₃ substrate. The fabricated hBN/β-Ga₂O₃ stack was used to fabricate an MIS-based Schottky junction device by depositing Ni and In metal electrodes, as shown in the schematic diagram (Figure 1b).

The fabricated Schottky junction with a configuration of Ni/hBN/β-Ga₂O₃/In was characterized, and the effect of the interfacial hBN layer was analyzed.

The as-received β-Ga₂O₃ sample was characterized using X-ray diffraction (XRD), UV-vis absorption spectroscopy, and Raman spectroscopy. The XRD studies were carried out using a Rigaku Smart Lab SE with Cu K α radiation as the X-ray source ($\lambda_{av} = 1.5406 \text{ \AA}$). A JEOL JSM 5600 scanning electron microscope at a voltage of 20 kV was used to examine the hBN-transferred β-Ga₂O₃ sample. An NRS 3300 laser Raman spectrometer was used to analyze the β-Ga₂O₃ sample at a laser excitation wavelength of 532.08 nm. Vertical Schottky junction

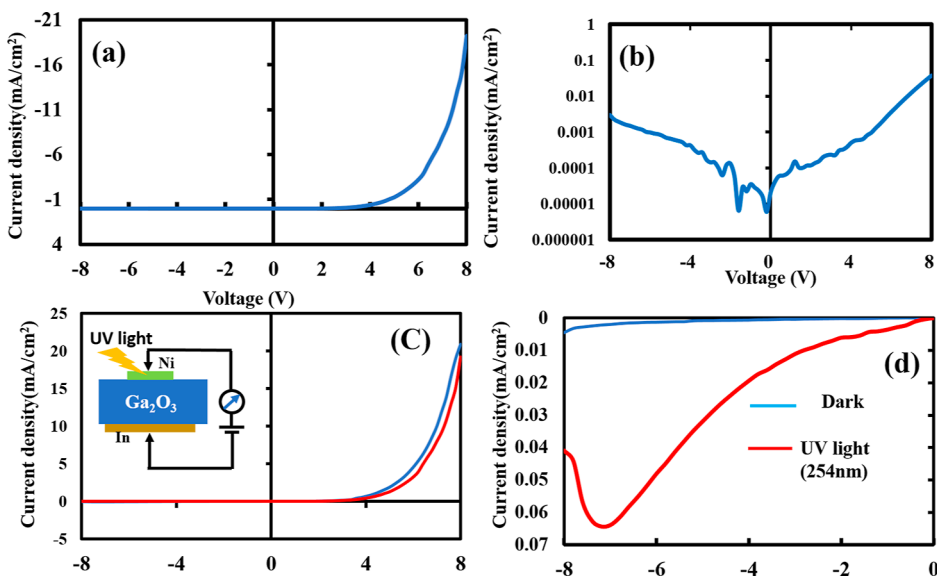


Figure 5. J – V characteristic of $\text{Ni}/\beta\text{-Ga}_2\text{O}_3$ 8 to -8 V: (a) J – V characteristics of forwarding bias voltage. (b) Log plot of the J – V curve. (c) J – V characteristics of the forward and reverse sweep of bias voltage. (d) Log plot of J – V curve dark and UV light at 254 nm.

devices were created by depositing Ni and In metal electrodes with the help of a metal mask. A metal mask with round-shaped holes (electrode area $\sim 0.003 \text{ cm}^2$) was used to deposit the top Ni electrode, whereas the In electrode was deposited on the backside of the $\beta\text{-Ga}_2\text{O}_3$ substrate almost covering the entire surface. The metal electrodes were deposited using the ULVAC VPC-260F thermal evaporator under high vacuum. The current density–voltage (J – V) measurements were carried out using a two-probe system and a Keithley 2401 source meter at room temperature. The deep-UV illumination measurement was performed using a UV lamp of 254 nm wavelength and a light intensity of $614 \mu\text{W}/\text{cm}^2$.

RESULTS AND DISCUSSION

Figure 2a shows the cross-sectional image of the hBN and $\beta\text{-Ga}_2\text{O}_3$ heterostructure with the Schottky junction. A barrier layer for the $\beta\text{-Ga}_2\text{O}_3$ Schottky junction can be formed by an hBN layer with a high band gap (6.0 eV) and a suitable dielectric constant. The XRD spectra of the free-standing $\beta\text{-Ga}_2\text{O}_3$ substrate are shown in Figure 2b. A strong diffraction peak at 61.01 cm^{-1} corresponding to the (020) reflection phase of $\beta\text{-Ga}_2\text{O}_3$ was observed for the sample. The XRD spectra are shown in the JCPD card number 06-0246.⁴¹ Figure 2c shows a scanning electron microscopy (SEM) image for the transferred hBN layer on the $\beta\text{-Ga}_2\text{O}_3$ substrate.

The transferred hBN film on the $\beta\text{-Ga}_2\text{O}_3$ substrate remains intact due to van der Waals interaction; however, SEM analysis revealed the formation of a wrinkle in the hBN thin film and surface impurities. Generally, such a type of wrinkle formation is observed for the large-area-transferred hBN film synthesized by a CVD process. The Raman spectra of the $\beta\text{-Ga}_2\text{O}_3$ sample are shown in Figure 2d, with a high-intensity Raman peak at 200 cm^{-1} for the Ag Raman mode, indicating the high-quality crystalline nature of the $\beta\text{-Ga}_2\text{O}_3$ sample used for device fabrication. The mid- and high-frequency Raman peaks are at around 354, 424, 486, 640, and 657 cm^{-1} , corresponding to distortion of Ga_2O_6 octahedra and the stretching/bending of the GaO_4 tetrahedra, respectively, as also discussed in previous reports.^{41,42} These analyses show a successful transfer of the CVD-synthesized hBN film on the bulk $\beta\text{-Ga}_2\text{O}_3$ substrate.

The hBN/ $\beta\text{-Ga}_2\text{O}_3$ sample was further studied by X-ray photoelectron spectroscopy (XPS) analysis.

Figure 3 shows the XPS analysis for the hBN/ $\beta\text{-Ga}_2\text{O}_3$ sample, presenting the elemental composition. Figure 3a shows the B 1s XPS spectrum for the hBN/ $\beta\text{-Ga}_2\text{O}_3$ heterostructure with a peak center at 192 eV. Similarly, Figure 4b shows the N 1s XPS spectra for the hBN film on a $\beta\text{-Ga}_2\text{O}_3$ substrate with a peak center at 400.1 eV. Again, Figure 3c shows the Ga 3d peak with a peak center at around 22.3 eV for the $\beta\text{-Ga}_2\text{O}_3$ sample. The XPS peak for the $\beta\text{-Ga}_2\text{O}_3$ was obtained considering the thin hBN film for the fabricated hBN/ $\beta\text{-Ga}_2\text{O}_3$ heterostructure. Figure 3d shows the split Ga 2p peaks, where Ga 2p_{1/2} and Ga 2p_{3/2} peaks are obtained at 1119 and 1144.8 eV, respectively. The chemical structures of the hBN/ $\beta\text{-Ga}_2\text{O}_3$ heterostructure were confirmed by XPS analysis, with the transferred CVD-synthesized hBN film remaining intact and stable on the $\beta\text{-Ga}_2\text{O}_3$ substrate surface. The current–voltage properties of the hBN/ $\beta\text{-Ga}_2\text{O}_3$ heterostructure Schottky junction were studied.

Figure 4a shows the J – V characteristics for the device with a voltage range of -2 to 2 V. The inset of Figure 4a shows the schematic diagram for the fabricated $\text{Ni}/\beta\text{-Ga}_2\text{O}_3/\text{In}$ Schottky junction device. Figure 4b shows the logarithmic plot for the J – V characteristics. The J – V characteristics indicate that a suitable Schottky junction formation for the $\text{Ni}/\beta\text{-Ga}_2\text{O}_3$ contact has occurred. Figure 4c depicts the forward and reverse sweeps with a bias voltage ranging from -2 to 2 V. For the forward bias voltage, the measured J – V curve revealed no hysteresis effect. Figure 4d depicts the J – V characteristics with and without deep-UV light illumination (254 nm). A dark current of $0.00074 \text{ mA}/\text{cm}^2$ was enhanced to $0.0115 \text{ mA}/\text{cm}^2$ at a reverse bias voltage of 2 V, under the illumination of 254 nm wavelength and a power of $614 \mu\text{W}/\text{cm}^2$. The photo-responsivity of $\text{Ni}/\beta\text{-Ga}_2\text{O}_3$ was calculated. At a reverse bias voltage of 2 V, the current density in a Schottky junction device is 16.28 mA/W . At lower bias voltages, the photo-responsivity of the fabricated device is not considered high; however, the photo-responsivity increases with increasing reverse bias voltage.⁴⁷

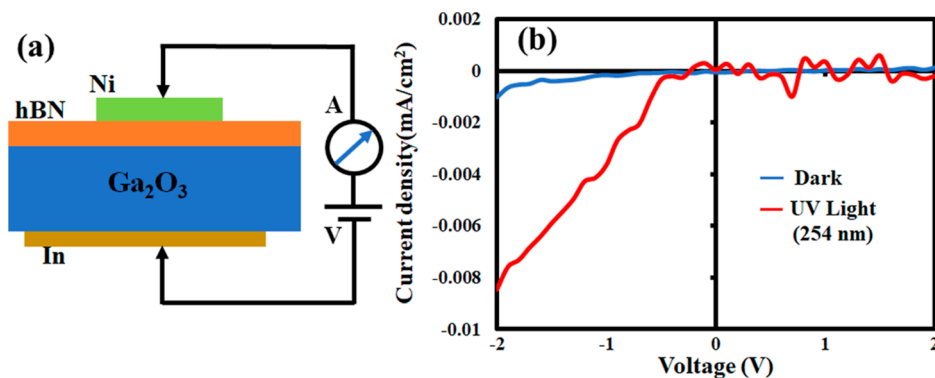


Figure 6. (a) Schematic diagram of the fabricated Ni/hBN/β-Ga₂O₃/In Schottky junction. (b) J – V characteristics of the device for a voltage range of 2 to -2 V.

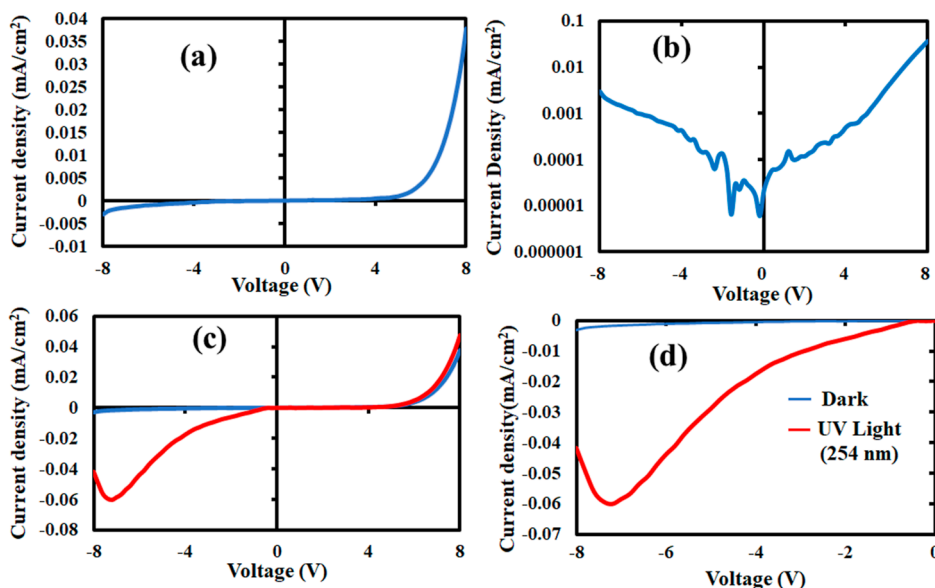


Figure 7. (a) J – V characteristics of the Ni/hBN/β-Ga₂O₃/In Schottky junction device for the voltage range of -8 to 8 V and (b) log plot of the J – V curve. (c) J – V characteristics with and without deep-UV illumination (254 nm) for bias voltage in the range of -8 to 8 V and (d) photoresponsivity at the reverse bias voltage (photoresponsivity of 95.11 mA/W at 7.2 V).

Figure 5 shows the J – V characteristics of the fabricated device with and without UV light illumination under -8 to 8 V. The forward turn-on voltage for the Ni/β-Ga₂O₃/In Schottky junction was obtained to be around 3.8 V. Figure 5a,b shows the J – V characteristic in the dark and the corresponding logarithmic plot for bias voltages ranging from -8 to 8 V. The J – V characteristics of the Ni/β-Ga₂O₃ Schottky junction, Figure 5c, depict a schematic of the fabricated device with a device structure of Ni/β-Ga₂O₃/In, the forward and reverse sweeps at bias voltages ranging from -8 to 8 V. For the forward bias voltage, the measured J – V curve revealed no hysteresis effect. Figure 5d depicts the J – V characteristics of an applied bias voltage ranging from -8 to 8 V under deep UV illumination (254 nm). Similarly, a dark current of 0.00208 mA/cm² was enhanced to 0.0643 mA/cm² at a reverse bias voltage of 7.2 V, under the illumination of 254 nm wavelength and a power density of 614 μ W/cm². The photoresponsivity is calculated to be 101.33 mA/W at 7.2 V reverse bias voltage for the constructed Ni/β-Ga₂O₃/In Schottky junction device.

Figure 6a shows a schematic diagram of the fabricated Ni/hBN/β-Ga₂O₃/In heterojunction Schottky junction device.

The CVD-synthesized hBN film was transferred on β-Ga₂O₃ by wet-etching the Cu foil with a support layer of PMMA. The Ni top electrode on the hBN/β-Ga₂O₃ heterojunction was deposited by thermal evaporation to configure a Schottky junction device. Figure 6b depicts the J – V characteristics of the fabricated device with and without deep-UV light illumination for a bias voltage range of -2 to 2 V (wavelength 254 nm). In contrast to the device fabricated without the hBN layer, the forward current did not increase as the bias voltage was increased up to 2 V. The hBN film with an ultrawide band gap can act as a barrier layer at the interface of Ni and β-Ga₂O₃. However, at the reverse bias voltage, photoresponsivity was measured, indicating the heterojunction device's sensitivity to deep-UV light.

Figure 7a shows the J – V characteristics of the Ni/hBN/β-Ga₂O₃/In Schottky junction device for the voltage range of -8 to 8 V. The forward turn voltage for the Ni/hBN/β-Ga₂O₃/In Schottky junction was obtained to be around 4.8 V, which is higher than that of the device with the hBN layer. It was also observed that the device's forward current was significantly low up to an applied voltage of 2 V. Figure 7b shows the corresponding logarithmic plot for the corresponding J – V

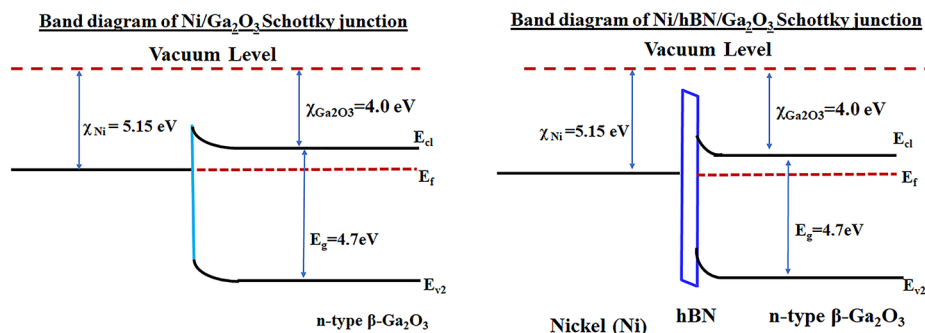


Figure 8. (a) Energy band diagram of the Ni/β-Ga₂O₃ Schottky junction vacuum level. (b) Band diagram of the Ni/hBN/β-Ga₂O₃/In Schottky junction vacuum level.

curve. Similarly, Figure 7c shows the *J*–*V* characteristics for the device with and without light illumination. Under the illumination of deep-UV light with a wavelength of 254 nm, a significant photoresponsivity can be observed in the reverse bias voltage. Figure 7d depicts the *J*–*V* curve in the reverse bias voltage range (0 to –8 V) used to measure photoresponsivity at a bias voltage. At 7.2 V bias, the photoresponsivity was 95.11 mA/W. The photoresponsivity is nearly identical to that of the device without the hBN layer; however, the forward turn-on voltage is higher, and the current density is lower. Turn-on voltage and forward current density differ significantly with and without the hBN layer on the β-Ga₂O₃, whereas photoresponsive reverse current density was nearly identical at an applied bias voltage of –7.2 V. Thus, a high photoresponsivity can be obtained in a Ni/hBN/β-Ga₂O₃/In-based heterojunction Schottky diode with high forward current turn-on voltage and low current density.

Figure 8a shows the energy band diagram for the Ni/β-Ga₂O₃ Schottky junction. The Ni metal contact with a higher work function (5.15 eV) forms a suitable Schottky potential with the n-type β-Ga₂O₃. A photoresponsivity was obtained at a reverse bias voltage for the illuminated deep-UV light considering the Schottky junction interface of Ni and Ga₂O₃. Similarly, Figure 8b shows the energy band diagram for the Ni/β-Ga₂O₃ Schottky junction, where the hBN layer acts as a barrier layer at the Ni and β-Ga₂O₃ interface.^{48,49} The *J*–*V* curve shows that the diode turn-on voltage increased, but no reduction in reverse saturation current was observed. The photoresponsivity of the Ni/hBN/β-Ga₂O₃/Schottky junction to the illuminated deep-UV light of wavelength 254 nm was 95.11 mA/W. Thus, the Ni/hBN/β-Ga₂O₃/In Schottky junction demonstrated that a significant photoresponsivity can be obtained with a tunable turn-on voltage and forward current. Our study showed that the interfacial hBN layer can be used as an insulating barrier layer for the fabrication of ultrawide band gap Schottky junction devices.⁴⁹

CONCLUSIONS

In conclusion, we have demonstrated the fabrication of a Ni/β-Ga₂O₃ Schottky junction device with an hBN interface layer. The hBN film was synthesized by CVD process and transferred on a free-standing β-Ga₂O₃ substrate by the wet chemical transfer method. XRD, Raman spectroscopy, and SEM analysis confirmed the hBN/β-Ga₂O₃ heterostructure of the Ga₂O₃ substrate and transferred hBN film. The *J*–*V* characteristics of a fabricated Schottky junction with and without the hBN interfacial layer were investigated. It was discovered that the hBN interfacial film significantly increases the turn-on voltage

for the forward current of the Ni/hBN/β-Ga₂O₃/In Schottky junction. Furthermore, the created Ni/hBN/β-Ga₂O₃/In Schottky junction showed a photoresponsivity of 95.11 mA/W for the illuminated deep-UV light of wavelength 254 nm. The hBN layer acts as a suitable barrier layer as demonstrated, where the turn-on voltage, forward current density, and photoresponsivity can be optimized for the Ni/β-Ga₂O₃ Schottky junction.

AUTHOR INFORMATION

Corresponding Authors

Venkata Krishna Rao Rama – Graduate School of Natural Science and Technology, Okayama University, Okayama 700-8530, Japan; orcid.org/0000-0001-9244-6250; Email: Krishnasrao20@gmail.com

Yasuhiko Hayashi – Graduate School of Natural Science and Technology, Okayama University, Okayama 700-8530, Japan; orcid.org/0000-0002-4113-5548; Phone: +81-86-251-8230; Email: hayashi.yasuhiko@okayama-u.ac.jp

Authors

Ajinkya K. Ranade – Department of Physical Science and Engineering, Nagoya Institute of Technology, Nagoya 466-8555, Japan

Pradeep Desai – Department of Physical Science and Engineering, Nagoya Institute of Technology, Nagoya 466-8555, Japan; orcid.org/0000-0001-9180-8395

Bhagyashri Todankar – Department of Physical Science and Engineering, Nagoya Institute of Technology, Nagoya 466-8555, Japan; orcid.org/0000-0001-8493-887X

Golap Kalita – Department of Physical Science and Engineering, Nagoya Institute of Technology, Nagoya 466-8555, Japan; Frontier Research Institute for Material Science, Nagoya Institute of Technology, Nagoya 466-8555, Japan

Hiroo Suzuki – Graduate School of Natural Science and Technology, Okayama University, Okayama 700-8530, Japan; orcid.org/0000-0002-1404-7374

Masaki Tanemura – Department of Physical Science and Engineering, Nagoya Institute of Technology, Nagoya 466-8555, Japan

Complete contact information is available at:
<https://pubs.acs.org/10.1021/acsomega.2c00506>

Notes

The authors declare no competing financial interest.

ACKNOWLEDGMENTS

We would like to thank Prof. Yoshifumi Yamashita and Prof. Takeshi Nishikawa for their continued support and suggestion on the manuscript. There is no funding for this research work to disclose.

REFERENCES

- (1) Tippins, H. H. Optical absorption and photoconductivity in the band edge of β -Ga₂O₃. *Phys. Rev.* **1965**, *140*, A316–A319.
- (2) Higashiwaki, M.; Sasaki, K.; Kuramata, A.; Masui, T.; Yamakoshi, S. Gallium oxide (Ga₂O₃) Metal-semiconductor field-effect transistors on single-crystal β -Ga₂O₃ (010) substrates. *Appl. Phys. Lett.* **2012**, *100*, 013504.
- (3) Xue, H. W.; He, Q. M.; Jian, G. Z.; Long, S. B.; Pang, T.; Liu, M. An overview of the ultra-wide bandgap Ga₂O₃ semiconductor-based Schottky barrier diode for power electronics application. *Nanoscale Res. Lett.* **2018**, *13*, 1–13.
- (4) Kalita, G.; Kobayashi, M.; Shaarin, M. D.; Mahyavanshi, R. D.; Tanemura, M. Schottky barrier diode characteristics of graphene-GaN heterojunction with hexagonal boron nitride interfacial layer. *Phys. Status Solidi A* **2018**, *215*, 1800089.
- (5) Yikai, L.; Zhaofu, Z.; Zhibin, G.; Qingkai, Q.; Mengyuan, H. Tunable properties of novel Ga₂O₃ monolayer for electronics and optoelectronics applications. *ACS Appl. Mater. Interfaces* **2020**, *12*, 30659–30669.
- (6) Higashiwaki, M.; Sasaki, K.; Murakami, H.; Kumagai, Y.; Koukitu, A.; Kuramata, A.; Masui, T.; Yamakoshi, S. Recent progress in Ga₂O₃ power devices. *Semicond. Sci. Technol.* **2016**, *31*, 034001.
- (7) Baldini, M.; Galazka, Z.; Wagner, G. Recent progress in the growth of β -Ga₂O₃ for power electronics applications. *Mater. Sci. Semicond. Process.* **2018**, *78*, 132–146.
- (8) Pearton, S. J.; Ren, F.; Tadjer, M.; Kim, J. Perspective: Ga₂O₃ for ultra-high power rectifiers and MOSFETs: Ga. *J. Appl. Phys.* **2018**, *124*, 220901.
- (9) Tomm, Y.; Reiche, P.; Klimm, D.; Fukuda, T. Czochralski grown Ga₂O₃ crystals. *J. Cryst. Growth* **2000**, *220*, 510–514.
- (10) Yuan, C.; Zhang, Y.; Montgomery, R.; Kim, S.; Shi, J.; Mauze, A.; Itoh, T.; Speck, J. S.; Graham, S. Modeling and analysis for thermal management in gallium oxide field-effect transistors. *J. Appl. Phys.* **2020**, *127*, 154502.
- (11) Galazka, Z.; Irmscher, K.; Uecker, R.; Bertram, R.; Pietsch, M.; Kwasniewski, A.; Naumann, M.; Schulz, T.; Schewski, R.; Klimm, D.; Bickermann, M. On the bulk β -Ga₂O₃ single crystals grown by the czochralski method. *J. Cryst. Growth* **2014**, *404*, 184–191.
- (12) Aida, H.; Nishiguchi, K.; Takeda, H.; Aota, N.; Sunakawa, K.; Yaguchi, Y. Growth of β -Ga₂O₃ single crystals by the edge-defined, film fed growth method. *Jpn. J. Appl. Phys.* **2008**, *47*, 8506–8509.
- (13) Ohira, S.; Yoshioka, M.; Sugawara, T.; Nakajima, K.; Shishido, T. Fabrication of hexagonal GaN on the surface of β -Ga₂O₃ single crystal by nitridation with NH₃. *Thin Solid Films* **2006**, *496*, 53–57.
- (14) Villora, E. G.; Shimamura, K.; Yoshikawa, Y.; Aoki, K.; Ichinose, N. Large-size β -Ga₂O₃ single crystals and wafers. *J. Cryst. Growth* **2004**, *270*, 420–426.
- (15) Kuramata, A.; Koshi, K.; Watanabe, S.; Yamaoka, Y.; Masui, T.; Yamakoshi, S. High-quality β -Ga₂O₃ single crystals grown by edge-defined film-fed growth. *Jpn. J. Appl. Phys.* **2016**, *55*, 1202A2.
- (16) Nikolaev, V. I.; Pechnikov, A. I.; Nikolaev, V. V.; Scheglov, M. P.; Chikirayaka, A. V.; Stepanov, S. I.; Medvedev, O. S.; Shapenkov, S. V.; Ubyivovik, E. V.; Vyvenko, O. F. HVPE growth of α -and ϵ -Ga₂O₃ on patterned sapphire substrates. *J. Phys.: Conf. Ser.* **2019**, *1400*, 055049.
- (17) Leach, J. H.; Udwary, K.; Rumsey, J.; Dodson, G.; Splawn, H.; Evans, K. R. Halide vapor phase epitaxial growth of β -Ga₂O₃ and α -Ga₂O₃ films. *APL Mater.* **2019**, *7*, 022504.
- (18) Nepal, N.; Scott Katzer, D.; Meyer, D. J. MBE growth and characterization of gallium oxide. *Gallium Oxide* **2019**, 31–46.
- (19) Ha, M.-T.; Kim, K.-H.; Kwon, Y.-J.; Kim, C.-J.; Jeong, S.-M.; Bae, S.-Y. Understanding thickness uniformity of Ga₂O₃ thin films grown by mist chemical vapor deposition. *ECS J. Solid State Sci. Technol.* **2019**, *8*, Q3206–Q3212.
- (20) Pearton, S. J.; Yang, J.; Cary, P. H.; Ren, F.; Kim, J.; Tadjer, M. J.; Mastro, M. A. A review of Ga₂O₃ materials, processing, and devices. *Appl. Phys. Rev.* **2018**, *5*, 011301.
- (21) Wu, C.; Guo, D. Y.; Zhang, L. Y.; Li, P. G.; Zhang, F. B.; Tan, C. K.; Wang, S. L.; Liu, A. P.; Wu, F. M.; Tang, W. H. Systematic investigation of the growth kinetics of β -Ga₂O₃ epilayer by plasma-enhanced chemical vapor deposition. *Appl. Phys. Lett.* **2020**, *116*, 072102.
- (22) Hadamek, T.; Posadas, A. B.; Al-Quaiti, F.; Smith, D. J.; McCartney, M. R.; Demkov, A. A. β -Ga₂O₃ on Si (001) Grown by plasma-assisted MBE with γ -Al₂O₃ (111) Buffer Layer: Structural Characterization. *AIP Adv.* **2021**, *11*, 045209.
- (23) Uno, K.; Ohta, M.; Tanaka, I. Growth mechanism of α -Ga₂O₃ on a sapphire substrate by mist chemical vapor deposition using acetylacetone gallium source solutions. *Appl. Phys. Lett.* **2020**, *117*, 052106.
- (24) Nishinaka, H.; Nagaoka, T.; Kajita, Y.; Yoshimoto, M. Rapid homoepitaxial growth of (010) β -Ga₂O₃ thin films via mist chemical vapor deposition. *Mater. Sci. Semicond. Process.* **2021**, *128*, 105732.
- (25) Mondal, A. K.; Ping, L. K.; Shazni Mohammad Haniff, M. A.; Mohd Sarjidan, M. A.; Goh, B. T.; Mohamed, M. A. Temperature dependence of ultrathin mixed-phase Ga₂O₃ films grown on the α -Al₂O₃ substrate via mist-CVD. *ACS Omega* **2022**, *7*, 2252–2259.
- (26) Pozina, G.; Hsu, C. W.; Abrikossova, N.; Kaliteevski, M. A.; Hemmingsson, C. Development of β -Ga₂O₃ layers growth on sapphire substrates employing modeling of precursors ratio in halide vapor phase epitaxy reactor. *Sci. Rep.* **2020**, *10*, 22261.
- (27) Moser, N.; Liddy, K.; Islam, A.; Miller, N.; Leedy, K.; Asel, T.; Mou, S.; Green, A.; Chabak, K. Toward high voltage radio frequency devices in β -Ga₂O₃. *Appl. Phys. Lett.* **2020**, *117*, 242101.
- (28) Bhattacharyya, A.; Ranga, P.; Saleh, M.; Roy, S.; Scarpulla, M. A.; Lynn, K. G.; Krishnamoorthy, S. Schottky barrier height engineering in β -Ga₂O₃ using SiO₂ interlayer dielectric. *IEEE J. Electron Devices Soc.* **2020**, *8*, 286–294.
- (29) Chatterjee, B.; Zeng, K.; Nordquist, C. D.; Singisetti, U.; Choi, S. Device-level thermal management of gallium oxide field-effect transistors. *IEEE Trans. Compon. Packag. Manuf. Technol.* **2019**, *9*, 2352–2365.
- (30) Jia, X.; Hu, H.; Han, G.; Liu, Y.; Hao, Y. Analytical model for the channel maximum temperature in Ga₂O₃ MOSFETs. *Nanoscale Res. Lett.* **2021**, *16*, 29.
- (31) Farzana, E.; Zhang, Z.; Paul, P. K.; Arehart, A. R.; Ringel, S. A. Influence of metal choice on (010) β -Ga₂O₃ Schottky diode properties. *Appl. Phys. Lett.* **2017**, *110*, 202102.
- (32) Chabak, K. D.; Walker, D. E.; Green, A. J.; Crespo, A.; Lindquist, M.; Leedy, K.; Tetlak, S.; Gilbert, R.; Moser, N. A.; Jessen, G. Sub-micron gallium oxide radiofrequency field-effect transistors. *IEEE MTT-S International Microwave Workshop Series on Advanced Materials Processes RF THz Applications IMWS-AMP*; IEEE, 2018; pp 1–3.
- (33) Hsieh, Y.-S.; Li, C.-Y.; Lin, C.-M.; Wang, N.-F.; Li, J. V.; Houng, M.-P. Investigation of metal-insulator-semiconductor diode with α -Ga₂O₃ insulating layer by liquid phase deposition. *Thin Solid Films* **2019**, *685*, 414–419.
- (34) Hu, Z.; Zhou, H.; Feng, Q.; Zhang, J.; Zhang, C.; Dang, K.; Cai, Y.; Feng, Z.; Gao, Y.; Kang, X.; Hao, Y. Field-plated lateral β -Ga₂O₃ Schottky barrier diode with high reverse blocking voltage of more than 3 kV and high DC power figure-of-merit of 500 MW/cm². *IEEE Electron Device Lett.* **2018**, *39*, 1564–1567.
- (35) Li, W.; Hu, Z.; Nomoto, K.; Zhang, Z.; Hsu, J. Y.; Thieu, Q. T.; Sasaki, K.; Kuramata, A.; Jena, D.; Xing, H. G. 1230 V β -Ga₂O₃ Trench schottky barrier diodes with an ultra-low leakage current of <1 μ A/cm². *Appl. Phys. Lett.* **2018**, *113*, 202101.
- (36) Qin, Y.; Li, L.; Zhao, X.; Tompa, G. S.; Dong, H.; Jian, G.; He, Q.; Tan, P.; Hou, X.; Zhang, Z.; Yu, S.; Sun, H.; Xu, G.; Miao, X.; Xue, K.; Long, S.; Liu, M. Metal-semiconductor-metal ϵ -Ga₂O₃ solar-

- blind photodetectors with a record-high responsivity rejection ratio and their gain mechanism. *ACS Photonics* **2020**, *7*, 812–820.
- (37) Hasan, M. N.; Swinnich, E.; Tang, Z.; Shin, S. H.; Kim, M.; Zhang, P.; Seo, J. H. Flexible Crystalline β -Ga₂O₃ solar-blind photodetectors. *J. Mater. Chem. C* **2020**, *8*, 14732–14739.
- (38) Harada, T.; Tsukazaki, A. Control of Schottky barrier height in Metal/ β -Ga₂O₃ junctions by insertion of PdCoO₂ Layers. *APL Mater* **2020**, *8*, 041109.
- (39) Malakoutian, M.; Song, Y.; Yuan, C.; Ren, C.; Lundh, J. S.; Lavelle, R. M.; Brown, J. E.; Snyder, D. W.; Graham, S.; Choi, S.; Chowdhury, S. Polycrystalline diamond growth on β -Ga₂O₃ for thermal management. *Appl. Phys. Express* **2021**, *14*, 055502.
- (40) Zhu, N.; Ma, K.; Xue, X.; Su, J. The formation and role of the SiO₂ oxidation layer in the 4H-SiC/ β -Ga₂O₃ interface. *Appl. Surf. Sci.* **2022**, *581*, 151956.
- (41) Venkata Krishna Rao, R.; Ranade, A. K.; Desai, P.; Kalita, G.; Suzuki, H.; Hayashi, Y. Temperature-dependent device properties of γ -CuI and β -Ga₂O₃ heterojunctions. *SN Appl. Sci.* **2021**, *3*, 796.
- (42) Kalita, G.; Mahyavanshi, R. D.; Desai, P.; Ranade, A. K.; Kondo, M.; Dewa, T.; Tanemura, M. Photovoltaic action in graphene-Ga₂O₃ heterojunction with deep-ultraviolet irradiation. *Phys. Status Solidi RRL* **2018**, *12*, 1800198.
- (43) Kim, J.; Mastro, M. A.; Tadjer, M. J.; Kim, J. Quasi-two-dimensional h-BN/ β -Ga₂O₃ heterostructure metal-insulator-semiconductor field-effect transistor. *ACS Appl. Mater. Interfaces* **2017**, *9*, 21322–21327.
- (44) Sharma, S.; Kalita, G.; Vishwakarma, R.; Zulkifli, Z.; Tanemura, M. Opening of triangular hole in triangular-shaped chemical vapor deposited hexagonal boron nitride crystal. *Sci. Rep.* **2015**, *5*, 1–9.
- (45) Sharma, K. P.; Sharma, S.; Khaniya Sharma, A.; Paudel Jaisi, B.; Kalita, G.; Tanemura, M. Edge controlled growth of hexagonal boron nitride crystals on copper foil by atmospheric pressure chemical vapor deposition. *CrystEngComm* **2018**, *20*, 550–555.
- (46) Rosmi, M. S.; Shinde, S. M.; Rahman, N. D. A.; Thangaraja, A.; Sharma, S.; Sharma, K. P.; Yaacob, Y.; Vishwakarma, R. K.; Bakar, S. A.; Kalita, G.; Ohtani, H.; Tanemura, M. Synthesis of uniform monolayer graphene on re-solidified copper from waste chicken fat by low pressure chemical vapor deposition. *Mater. Res. Bull.* **2016**, *83*, 573–580.
- (47) Guo, D.; Liu, H.; Li, P.; Wu, Z. W.; Wang, S.; Cui, C.; Li, C.; Tang, W. Zero-power-consumption solar-blind photodetector zero-power-consumption solar-blind photodetector based on β -Ga₂O₃/NSTO heterojunction. *ACS Appl. Mater. Interfaces* **2016**, *9*, 1619–1628.
- (48) Sun, H.; Torres Castanedo, C. G.; Liu, K.; Li, K.-H.; Guo, W.; Lin, R.; Liu, X.; Li, J.; Li, X. Valence and conduction band offsets of β -Ga₂O₃/AlN heterojunction. *Appl. Phys. Lett.* **2017**, *111*, 162105.
- (49) Zhou, X.; Zhang, L.; Zhang, X.; Ma, Y.; Wei, X.; Chen, T.; Tang, W.; Xu, K.; Zeng, Z.; Zhang, X.; Fu, H.; Zhang, B. Band alignment of ultrawide bandgap ε -Ga₂O₃/h-BCN heterojunction epitaxially grown by metalorganic chemical vapor deposition. *Appl. Surf. Sci.* **2022**, *583*, 152502.

□ Recommended by ACS

Epitaxial Stabilization of Complete Solid-solution β - $(\text{Al}_x\text{Ga}_{1-x})_2\text{O}_3$ (100) Films by Pulsed-laser Deposition

Ryo Wakabayashi, Akira Ohtomo, et al.

APRIL 08, 2021

CRYSTAL GROWTH & DESIGN

READ ▶

Band Offsets of the MOCVD-Grown β - $(\text{Al}_{0.21}\text{Ga}_{0.79})_2\text{O}_3/\beta\text{-Ga}_2\text{O}_3$ (010) Heterojunction

Timothy A. Morgan, Morgan E. Ware, et al.

JULY 18, 2022

ACS APPLIED MATERIALS & INTERFACES

READ ▶

Monolithic Epitaxial Integration of β -Ga₂O₃ with 100 Si for Deep Ultraviolet Photodetectors

Sandeep Vura, Srinivasan Raghavan, et al.

MARCH 26, 2022

ACS APPLIED ELECTRONIC MATERIALS

READ ▶

Piezotronic Effect Modulated Flexible AlGaN/GaN High-Electron-Mobility Transistors

Jiyuan Zhu, Zhong Lin Wang, et al.

OCTOBER 21, 2019

ACS NANO

READ ▶

Get More Suggestions >